LEGIBILITY NOTICE

A major purpose of the Technical Information Center is to provide the broadest dissemination possible of information contained in DOE's Research and Development Reports to business, industry, the academic community, and federal, state and local governments.

Although portions of this report are not reproducible, it is being made available in microfiche to facilitate the availability of those parts of the document which are legible.

3

LA-UR- 90-2851

SEP 07 1990

Alamos National Laboratory is operated by the University of California for the United States Department of Energy under contract W-7405-ENG-36

LA-UR--90-2851

DE90 016483

TITLE: DESIGN, PERFORMANCE, AND CALIBRATION OF THE ALEXIS ULTRASOFT X-RAY TELESCOPES

AUTHOR(S): Jeffrey J. Bloch, Frank Ameduri, William C. Priedhorsky, Diane Roussel-Dupre', and Barham W. Smith
Los Alamos National Laboratory
Oswald H. W. Siegmund, Scott Cully, John Warren, and Geoffrey A. Gaines
Space Sciences Laboratory, University of Caliiofnia/Berkeley

SUBMITTED TO: Proceedings of the Conference 1344, EUV X-Ray and Gamma-Ray Instrumentation for AStronomy for SPIE, San Diego, CA, July 8-13, 1990

DISCLAIMER

8/90

MASTER

Los Alamos National Laboratory
Los Alamos, New Mexico 87545

Design, Performance, and Calibration of the ALEXIS Ultrasoft X-ray Telescopes

Jeffrey J. Bloch, Frank Ameduri, William C. Priedhorsky, Diane Roussel-Dupre', and Barham W. Smith
Space Astronomy and Astrophysics Group
Los Alamos National Laboratory

Oswald H. W. Siegmund, Scott Cully, John Warren, and Geoffrey A. Gaines
Space Sciences Laboratory
University of California/Berkeley

ABSTRACT

The Array of Low Energy X-ray Imaging Sensors (ALEXIS) experiment consists of six wide angle EUV/ultrasoft X-ray telescopes utilizing normal incidence multilayer mirrors, flown on a miniature satellite to map out the sky in three narrow bandpasses around 66, 71, and 95 eV. The 66 and 71 eV bandpasses are centered on intense Fe emission lines which are characteristic of million degree plasmas such as the one thought to produce the soft X-ray background. The 95 eV bandpass has a higher throughput and is more sensitive to continuum sources. The mission will be launched into orbit on the Pegasus Air Launched Vehicle in mid-1991.

We will present the details of the ALEXIS telescope optical design, initial characterizations of the first flight mirrors and detectors, and the current schemes for characterizing and calibrating the completed telescope assemblies. We will also discuss the details of a novel "wavetrap" feature incorporated into the multilayer mirror structure to greatly reduce the mirror's reflectivity at 304Å, a major background contamination flux of He II emission from the geocorona.

1. INTRODUCTION

The ALEXIS (Array of Low-Energy X-Ray Imaging Sensors) satellite[1] is an ultrasoft X-ray monitor experiment that consists of six compact normal-incidence telescopes operating in narrow bands centered on 66, 71, and 95 eV (see Figure 1). The ALEXIS satellite and experiment are funded by DOE, and are being built as a collaboration between Los Alamos and Sandia National Laboratories (LANL, SNL), and Space Sciences Laboratory/UC Berkeley (SSL/UCB). The six ALEXIS telescopes are arranged in pairs and cover three overlapping 33° fields-of-view. During each 30-second spin of the satellite, ALEXIS will monitor the entire anti-solar hemisphere. Each telescope consists of a Mo-Si layered synthetic microstructure (LSM) spherical mirror, a prime focus curved profile microchannel plate detector with a wedge and strip readout, background-rejecting filters and magnets, and image processing readout electronics. The geometric area of each ALEXIS telescope will be about 25 cm^2, with spherical aberration limited resolution of about 1/2°. With the mirror, filter, and detector efficiencies folded in, the effective collecting area for an on-axis point source at the peak of each telescope's response function should be between 0.5 and 0.2 cm^2. Employing initial estimates of mirror reflectivities, detector quantum efficiencies, and filter transmissions, the 5 sigma survey sensitivity is estimated to be several x 10^{-3} photons cm^{-2} s^{-1} for line emission at the center of the bandpass. The spacecraft is a custom, low-cost, miniature satellite compatible with several expendable launch vehicles. The Air Force Space Test Program will launch ALEXIS via a Pegasus air-launched vehicle into a 400 nautical mile polar orbit scheduled for mid-1991.

The ALEXIS experiment weighs 100 pounds, draws 45 watts, and produces 10 kilobits/second of data. Position and time of arrival are recorded for each detected photon. ALEXIS will always be in a survey-monitor mode, with no individual source pointings. It is well-suited for simultaneous observations with ground-based observers who prefer to observe sources at opposition. Coordinated observations need not be arranged before the fact, because all sources in the anti-Sun hemisphere will be observed and archived. ALEXIS will be tracked from a single ground station in Los Alamos. Between ground station passes, data are stored in an on-board solid state memory of 72 Mbytes.

ALEXIS, with its wide fields-of-view and well-defined wavelength bands, will complement the upcoming NASA Extreme Ultraviolet Explorer and ROSAT EUV Wide Field Camera, which are sensitive broad-band survey experiments. ALEXIS will pursue a number of scientific objectives including: mapping the diffuse background in three emission line bands with the highest angular resolution to date[2], performing a narrow-band survey of point sources, searching for transient phenomena in the ultrasoft X-ray band, and providing synoptic monitoring of variable ultrasoft X-ray sources such as cataclysmic variables and flare stars. Unlike other ultrasoft X-ray experiments, the 66 and 71 eV ALEXIS bandpasses are tuned to the Fe IX-XII emission line complex. This set of emission lines is characteristic of million degree optically thin plasmas which exist in the coronae of stars and which are thought to fill a large fraction of interstellar space around the sun, creating the soft X-ray background.

2. GEOMETRICAL OPTICS

Normal incidence multilayer X-ray/EUV telescopes have been used for solar observations[3], but ALEXIS will be the first time they will be used for non-solar cosmic ultrasoft X-ray/EUV measurements. Figure 2 shows a cross sectional view of an ALEXIS telescope. It is an extremely simple optical design, consisting of an annular entrance aperture, an f/1 spherical mirror, an optical and UV rejecting filter, and a curved, microchannel plate detector with wedge and strip anode readout. The curved front of the microchannel plate follows the curvature of the focal surface so that the spatial resolution of the system is approximately constant over the entire 33° field-of-view. Spherical aberration limits the system's spatial resolution to about 0.5°. The hole in the spherical mirror covers an area that incoming rays never see and has several beneficial features. It provides some weight savings, a way to examine a flight filter in place, and a way to directly illuminate the detector for flat field tests or UV "scrubbing" operations.

We have constructed a computer model of this system and performed a set of raytrace calculations for one of these telescopes. The bottom of Figure 3 shows the shape of the point response function at increasing off-axis angles. The top of Figure 3 shows the geometric collecting area as a function of off-axis-angle. The effect of incoming rays being blocked by the detector body at larger off axis angles is evident in both the changing shape of the point response and the smaller amount of collecting area. At the largest off-axis angles, some of the incoming rays that are not blocked by the detector also fall off the edge of the mirror, further reducing the collecting area at the edge of the field of view.

In computing a telescope's performance as a function of wavelength, the important parameters for each ray that hits the detector are 1) the angle the ray reflects off of the mirror, 2) the angle the ray traverses the filter, and 3) the angle with respect to the microchannel plate pore axis that the ray strikes the detector. Parameters of secondary importance are the positions that each ray strikes the mirror and detector. In fact, the joint distribution of all of these variables for each incident ray must be considered in computing the final performance.

The reflectivity of the mirror at a given wavelength is a strong function of the angle with which the ray bounces off of the mirror. This is due to the nature of the interference reflection character of the multilayer that covers the mirror surface. We have computed the contributions to the total area-solid angle product ($A^*\Omega$) as a function of glancing angle reflection. This result is shown in Figure 4. Notice that we only have to consider angles between 72° and 78°. To determine the mirror's contribution to the telescope's total $A^*\Omega$ as at a given wavelength, this curve must be multiplied by the multilayer's reflectivity at each angle and the result integrated. Figure 5 shows the result of this calculation for each of the three bandpasses using models of the original target multilayer designs.

As has been shown previously[5,6], the quantum efficiency of a microchannel plate detectors is not only dependent on wavelength, but also the angle between the incoming ray and the axis of the microchannel plate pores. It is therefore necessary to know the distribution of the incoming ray angles with respect to the pores. This calculation was carried out using our simulation code and the result is shown in Figure 6. Because the microchannel plate pores are parallel to the optical axis, this distribution also reflects the way rays traverse the filter in front of the detector. When this curve is multiplied by the quantum efficiency vs. input angle curves for a detector at a given wavelength and integrated, an effective quantum efficiency for the telescope over the entire field of view is obtained. A similar calculation can be performed for the filter to obtain an effective filter transmission at a given wavelength.

In truth, these angle distribution curves are not independent of each other so the final computation of each telescope's performance will involve computing for each calculation ray the effects of the mirror reflectivity, filter transmission, and detector quantum efficiency.

3. MULTILAYER MIRRORS

Our progress developing the ALEXIS flight Mo-Si multilayer mirrors as well as the EUV mirror calibration facility at Los Alamos has been described previously[7,8]. As of this writing, we have obtained from our subcontractor, Ovonic Synthetic Materials Company, Inc. (OSMC), an initial set of 11 flight mirrors for ALEXIS and an attendant flat witness sample for each. The flat witness mirrors are 4 cm diameter quartz flats placed in the flight mirror holes at the time of deposition. At this time we are still evaluating the mirrors' performance and are attempting to understand some difficulties with the 304Å "wavetrap" feature of the mirror's design.

The fabrication of the ALEXIS mirrors has proved to be a significant technological challenge for several reasons. First, the surface of the mirrors is highly curved (diameter = 12.8 cm, radius of curvature = 13.52 cm) which makes it difficult

to put down a uniform multilayer structure over the entire diameter. We had an initial specification for ≤±1% variation in the multilayer d-spacing over the entire surface. OSMC arrived at a deposition process that substantially met our specification. All 11 flight mirrors received to date have uniformities over their entire diameters within ±1-2%. As of this writing, detailed spatial uniformity reflectivity measurements are in progress on all of the flight mirrors. Figure 7 shows the reflectivity data obtained from one of the flight 66eV bandpass mirrors measured with 186Å X-rays at several radii on the mirror.

The second challenge was to get the thickness of the Mo-Si layers correct in order to obtain the maximum reflectivities, within the wavelength band of interest, between glancing angles 72° and 78°, as discussed in section 2 above. This was perhaps most critical for the 71 eV bandpass mirrors where a significant spacing error could put the majority of the telescope's response at energies higher than the absorption edge of the aluminum filters used with the 71 and 66 eV bandpass telescopes, thus wiping out the telescope's sensitivity. Satisfactory layer spacings were obtained after several deposition iterations. It proved feasible to deposit a second and in some cases a third multilayer structure over the original coating when the first results were not satisfactory.

The third challenge was to put the correct recipe for the two Mo-Si layer pairs on top of the multilayer structure comprising the 304Å "wavetrap". One of the problems for astronomical instrumentation working in the EUV or ultrasoft X-ray regime is the intense EUV background from He II in the geocorona at 304Å. This background signal can be as much as 13 Rayleighs, or more than one million times stronger than signals of astrophysical interest in the 200 - 100Å region of the spectrum. Filtration can be used to block this background, but at a significant expense to the telescope's throughput at the wavelengths of interest. We realized that if the mirror's reflectivity at 304Å could be reduced without seriously degrading the mirror's performance in the telescope bandpass, the filters could be thinner and as much as 25% in instrument sensitivity could be regained.

Because 304Å radiation penetrates much less into the multilayers than radiation at the target wavelengths, the ALEXIS multilayer designs use the top two Mo-Si layer pairs to form an anti-reflection coating for 304Å radiation. The thickness of the two top layers were adjusted until a destructive interference condition was met for the 304Å light within the 72°-78° angle range that rays reflect from the mirror. The spacings for the rest of the 40 to 60 Mo-Si layer pairs beneath these were adjusted to constructively reflect the wavelengths in the telescope's bandpass. Reflectivity calculations for this type of multilayer configuration showed that we would retain high reflectivities (30-50%) at the peak of the desired bandpass and could have reflectivities as low as 10^{-6} at 304Å. More than a year was spent experimentally verifying this concept on flat mirror samples. Because all of the data (Cu-K diffractometry, reflectivity measurements at 186, 170, 130, 256, and 304Å, and Auger analysis) at our disposal did not fit a single model[4,10,11] of the multilayer structure, final adjustments to the recipes for the layer spacings were achieved empirically.

For the flight mirrors, reflectivities at 304Å of 10^{-4} or less have been achieved while performances in the main bandpasses have been in the 30-50% range, depending on the bandpass. An example of a 66 eV bandpass mirror's reflectivity performance at 304Å is shown in Figure 7.

However, the reflectivity at 304Å of all of the flight mirrors has varied with time. Some mirror's performance has gotten better (i.e. lower 304Å reflectivity) and others have gotten worse. The reflectivities at the bandpass wavelengths have not changed. The mirrors were stored in sealed plastic bag containers filled with dry nitrogen which had previously been shown to be a stable storage environment for flat wavetrap multilayer samples. As of this writing, we are still evaluating whether the changes are due to 1) surface contamination buildup, or 2) oxide or nitride formation at the surface. Diffusion of the Mo layers into the Si layers seems to be ruled out since models show that that process can never improve the performance of the wavetrap effect.

4. DETECTORS AND FILTERS

Calibration of the first set of flight ALEXIS filters is underway at SSL-UCB at the time of this writing. The current 66 and 71 eV bandpass telescope filters are comprised of 1200Å of aluminum and 600Å of carbon. The 95 eV bandpass telescope filters are made of 1500Å of Lexan, 200Å of titanium, and 900Å of boron. This first filter set was optimized using the initial encouraging results of the mirror wavetrap performances described above. If the current problems with the 304Å rejection capability of the mirrors can not be resolved, we will obtain a second thicker set of Aluminum/Carbon filters which will make up for the loss of background rejection by the 66 and 71 eV bandpass mirrors. The 95eV bandpass performance is not as susceptible to the degraded wavetrap operation because the Lexan/Titanium/Boron filter is more efficient in removing the 304Å background.

3. A. B. C. Walker, Jr., T. W. Barbee, Jr., R. B. Hoover, and J. F. Lindblom, "Sof: X-Ray Images of the Solar Corona with a Normal Incidence Cassegrain Multilayer Telescope", Science, 241, 1781-1787 (1987).

4. M. Born and E. Wolf, Principles of Optics, Pergamon Press, London (1959).

5. O.H.W. Siegmund, E. Everman, J.V. Vallerga, and M. Lampton, "Extreme ultraviolet quantum efficiency of opaque alkali halide photocathodes on microchannel plates", Proceedings of SPIE 868, 18-24, (1987).

6. G. W. Fraser, X-ray Detectors in Astronomy, Cambridge University Press, Cambridge (1989).

7. B. W. Smith, J. J. Bloch, D. Roussel-Dupre', "Metal multilayer mirrors for EUV/ultrasoft x-ray wide-field telescopes", Opt. Eng., 29(6), 592-596, (1990).

8. B. W. Smith, J. J. Bloch, D. Roussel-Dupre', "Metal multilayer mirrors for EUV/ultrasoft x-ray wide-field telescopes", SPIE conference on X-ray/EUV Optics for Astronomy and Microscopy, R. B. Hoover ed., Proc. SPIE 1160 (1989).

9. O. H. W. Siegmund, W. C. Priedhorsky, "Highly Curved Microchannel Plate Detectors", this conference.

10. D. L. Windt, thesis, U. Colorado (1987).

11. E. B. Palik, Handbook of Optical Constants, Academic Press, New York (1985).

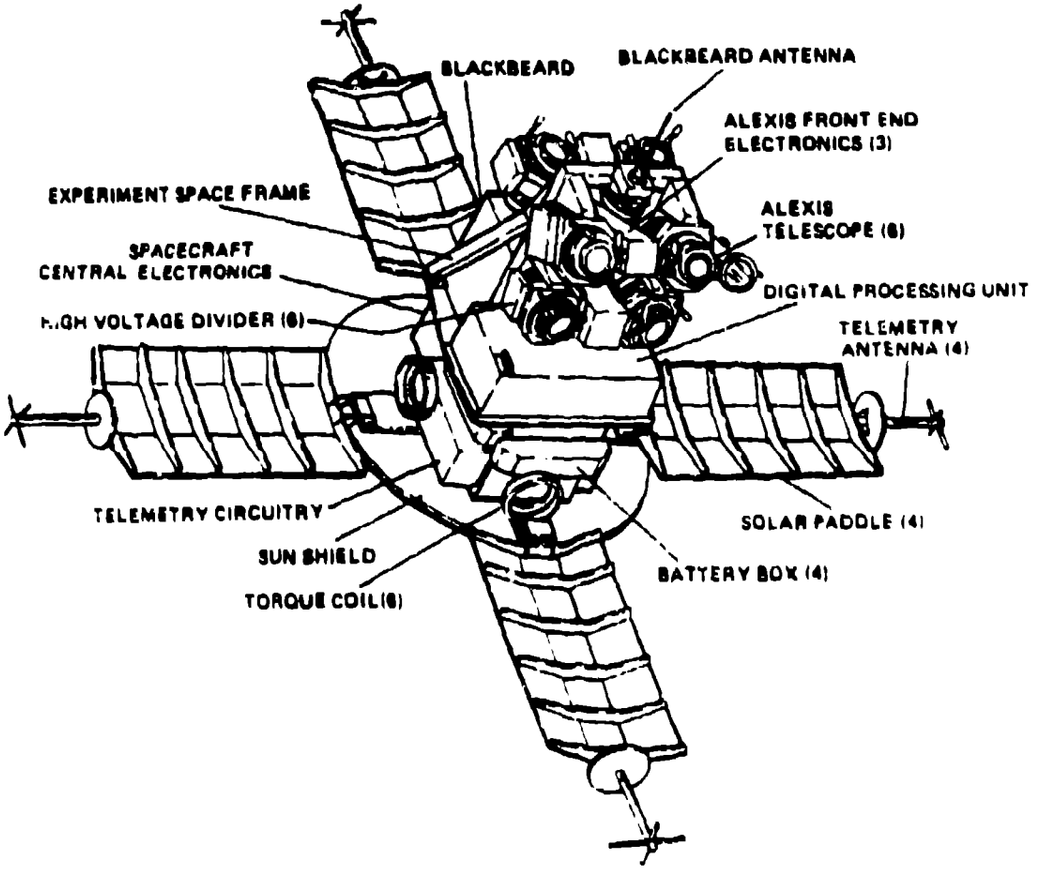

Figure 1 - Schematic diagram of the ALEXIS spacecraft.

SSL/UCB has built and calibrated the first ALEXIS flight detector and has delivered it to LANL for telescope integration. The characteristics of the curved microchannel plates used for the ALEXIS detectors are discussed elsewhere in this conference[9]. A unique feature incorporated into the ALEXIS detector design is a small circular mask placed permanently over a small part of the front of the detector at the edge of the active area. The mask shields a section of the detector from any incident EUV radiation. Thus any events located within that area arise from intrinsic dark counts or high energy particles. The event rate in this area will be used as an on-orbit monitor of high energy particle induced events. Calibrations with radioactive sources on the ground will determine the relationship between particle induced events under the mask and over the rest of the detector. This kind of background monitoring will be essential in analyzing the flux from diffuse sources of EUV emission.

Figure 8 shows that detector's quantum efficiency (QE) calibration for radiation incident at 15° to the pore axis. The error bars include the measurement errors as well as the uncertainty in the absolute calibration of the photodiode used as a standard. Figure 9 has several plots showing the relative change in QE at fixed wavelengths as a function of incident angle with respect to the microchannel plate pores.

The uniformity of the detector's spatial response was tested by placing a mask with a grid of pinholes with 2mm separation and 10μ diameters in front of the detector. The mask and detector were illuminated by UV light at a slight off-axis angle. The resulting image is shown in Figure 10. Figure 11 is a count histogram cross section across one of the pinhole rows. These tests indicate that the detector's spatial resolution is still well below the optical resolution of the telescopes.

5. TELESCOPE CALIBRATION FACILITY

The first step in assembling an ALEXIS telescope will be to position the detector properly with respect to the telescope optical axis. An optical bench setup is used to adjust the detector tilt. First a laser beam is centered on the optical axis of the telescope body. Then adjustments in the detector mounting spider are made until the laser bouncing off of the microchannel plate surface retroreflects back onto itself. A second optical bench setup is then used to adjust the position of the mirror for best focus. A wide collimated beam of laser light forms a spot on the surface of the detector. The spot is examined with a microscope and the mirror position is adjusted for what appears to be best focus. The telescope is also tilted back and forth to examine the off-axis focus. Any problems with the initial adjustment of the detector location within the telescope body should appear during this check.

Once the mirror and detector are fixed within the telescope body, the unit (without the filter) is placed in a vacuum chamber depicted in Figure 12. This setup will be used to further check the focus of the telescope as well as map out the relationship between X-Y location of events on the detector and the direction of the incoming rays. The gimbals on which the telescope is mounted are manipulated by two computer controlled motors. This entire test will be automated and controlled by a SUN workstation.

The final tests for throughput through the telescope system will be performed by a pencil beam test depicted in Figure 13. After the previous spatial mapping calibration, the flight filter is placed on the detector and the unit is re-assembled. It is then placed back in the gimbal mount, and the gimbal vacuum chamber is placed on a port of the LANL EUV reflectometry system. A monochromatic pencil beam of calibrated intensity is then directed into the entrance aperture of the telescope. The telescope can be maneuvered to different angles so that the pencil beam can traverse different paths through the telescope. The resulting output from the telescope is compared with calculations to determine the final model of telescope performance as a function of wavelength.

6. ACKNOWLEDGEMENTS

This work was performed under the auspices of the U.S. Department of Energy. We would like to thank James L. Wood and Rick Paparella of Ovonic Synthetic Materials Company, Inc. for helpful discussions and for providing the results of Cu-Kα diffractometry and AES measurements of the prototype mirrors.

7. REFERENCES

1. W. C. Priedhorsky, J. J. Bloch, B. W. Smith, K. Strobel, M. Ulibarri, J. Chavez, E. Evans, O. H. W. Siegmund, H. Marshall, J. Vallerga, and P. Vedder, "ALEXIS: An Ultrasoft X-Ray Monitor Experiment Using Miniature Satellite Technology", in X-Ray Instrumentation in Astronomy II, Proc SPIE 982 (1988).

2. J. J. Bloch and B. W. Smith, "The ALEXIS Project and the Local Interstellar Medium," in Proceedings of the Berkeley Colloquium on Extreme Ultraviolet Astronomy, R. Malina, ed., in press.

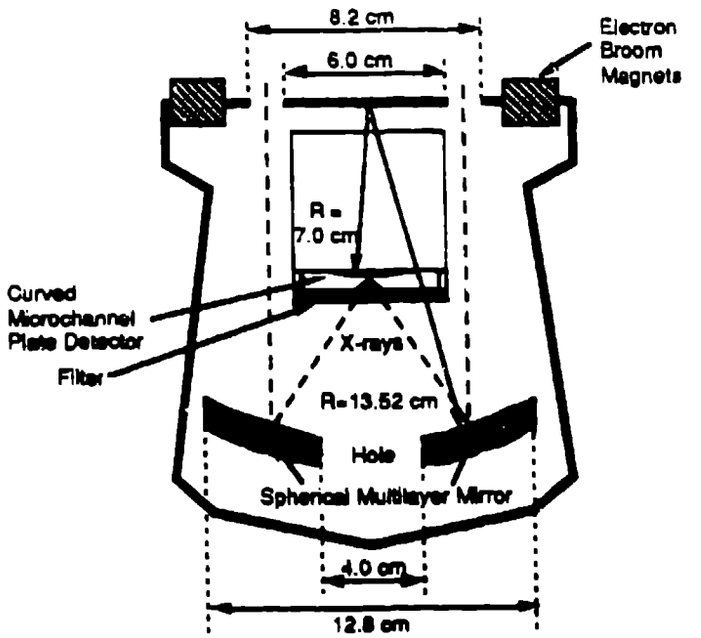

Figure 2. Cross sectional diagram of an ALEXIS telescope.

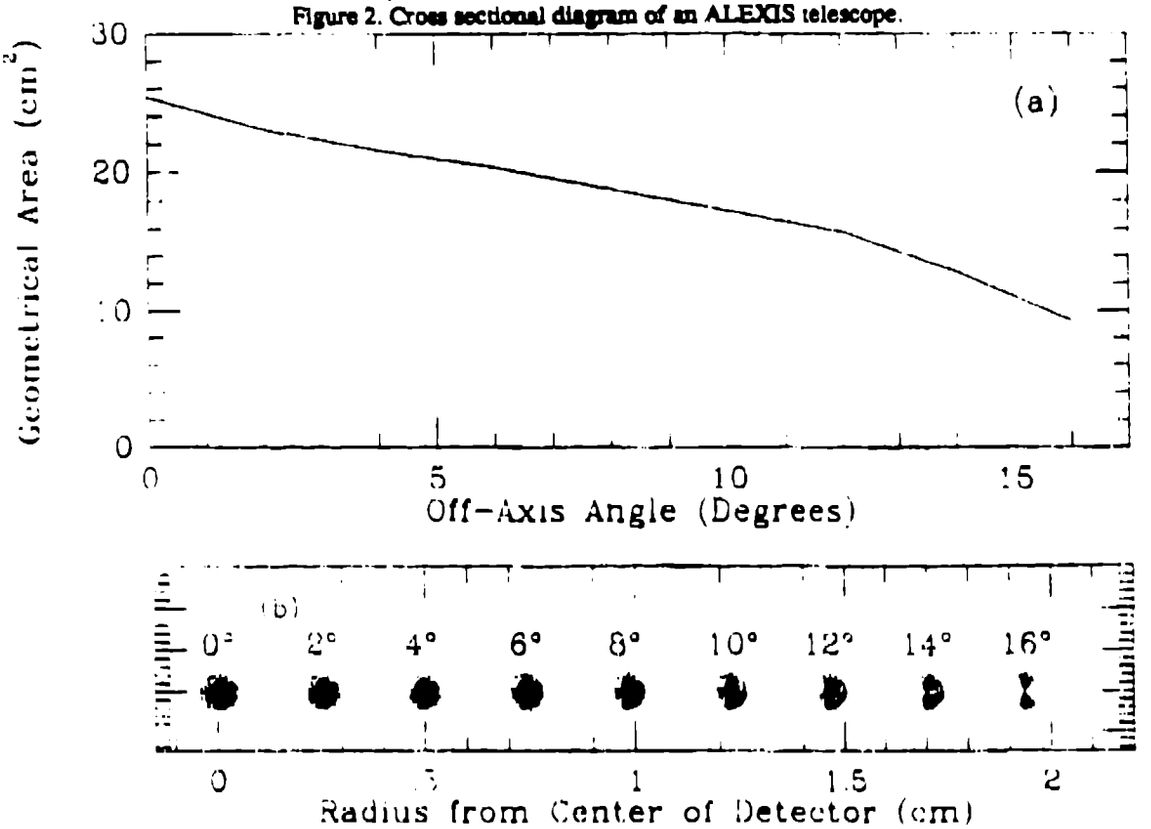

Figure 3. Computer raytrace calculations of the geometrical optics properties of an ALEXIS telescope. a) Geometric collecting area as a function of off-axis angle. b) Point response function as a function of off-axis angle.

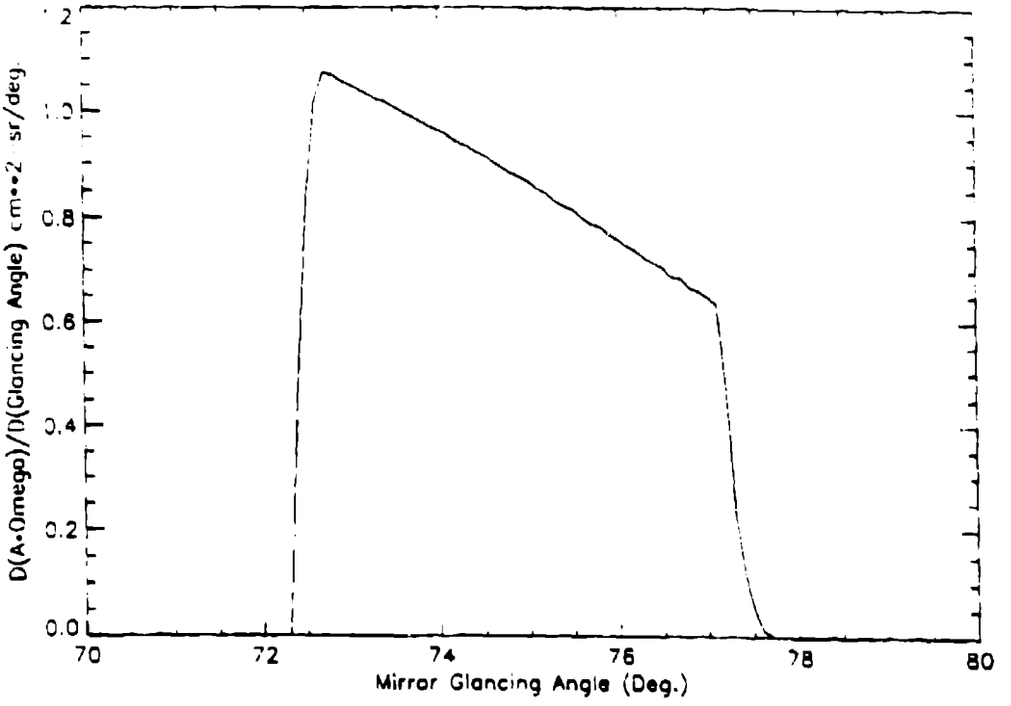

Figure 4 - Differential contributions to the total geometrical area-solid angle product(A*Ω) of the telescope as a function of different mirror glancing reflection angles. Note that 90° is normal incidence on this plot.

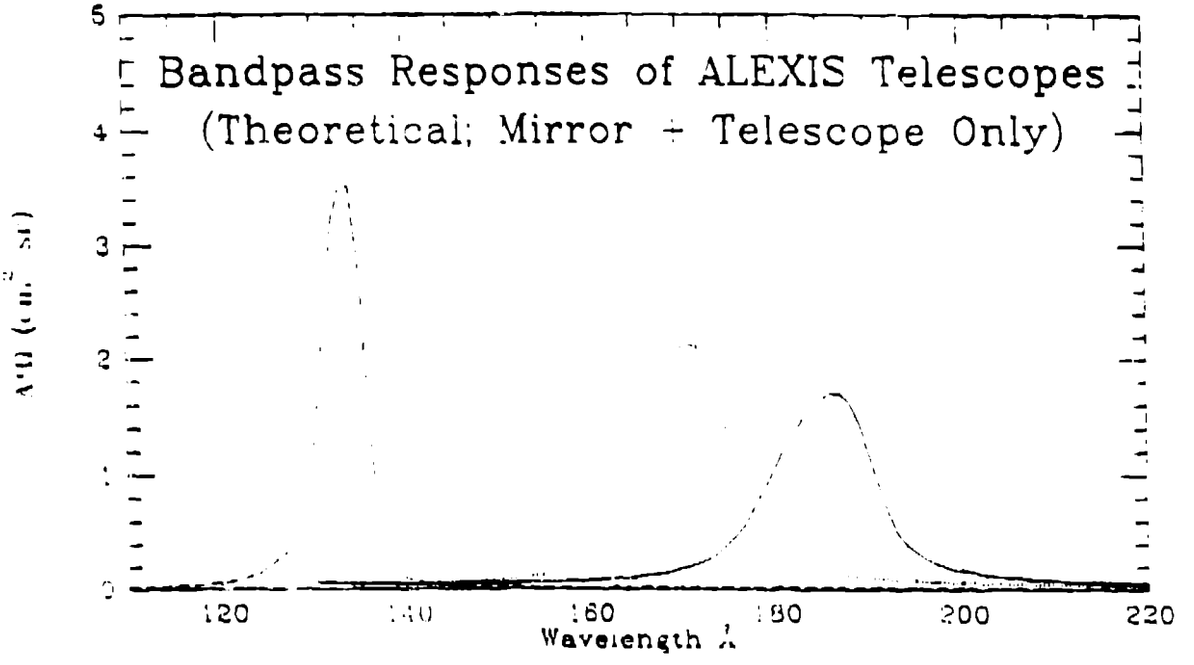

Figure 5. - Effective area-solid angle product (A*Ω) contribution from the multilayer mirror only for each ALEXIS bandpass as a function of wavelength. The filter transmission and detector quantum efficiencies have not been folded into these curves.

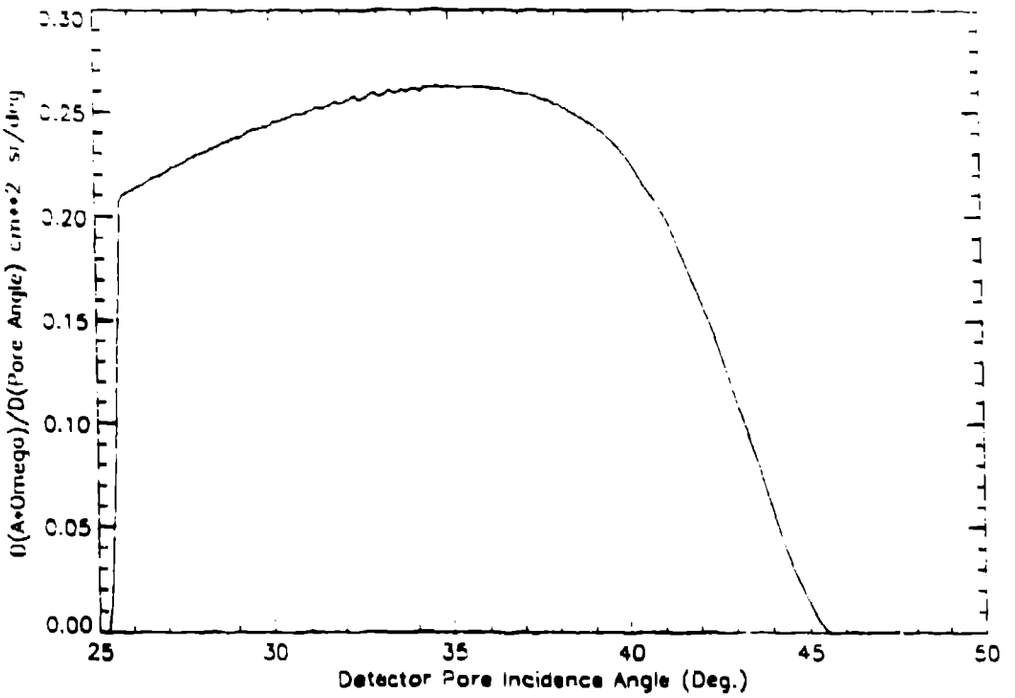

Figure 6 - Computed differential contributions to the total area-solid angle product (A*Ω) as a function of the angle rays hit the detector surface with respect to the microchannel plate pore axes.

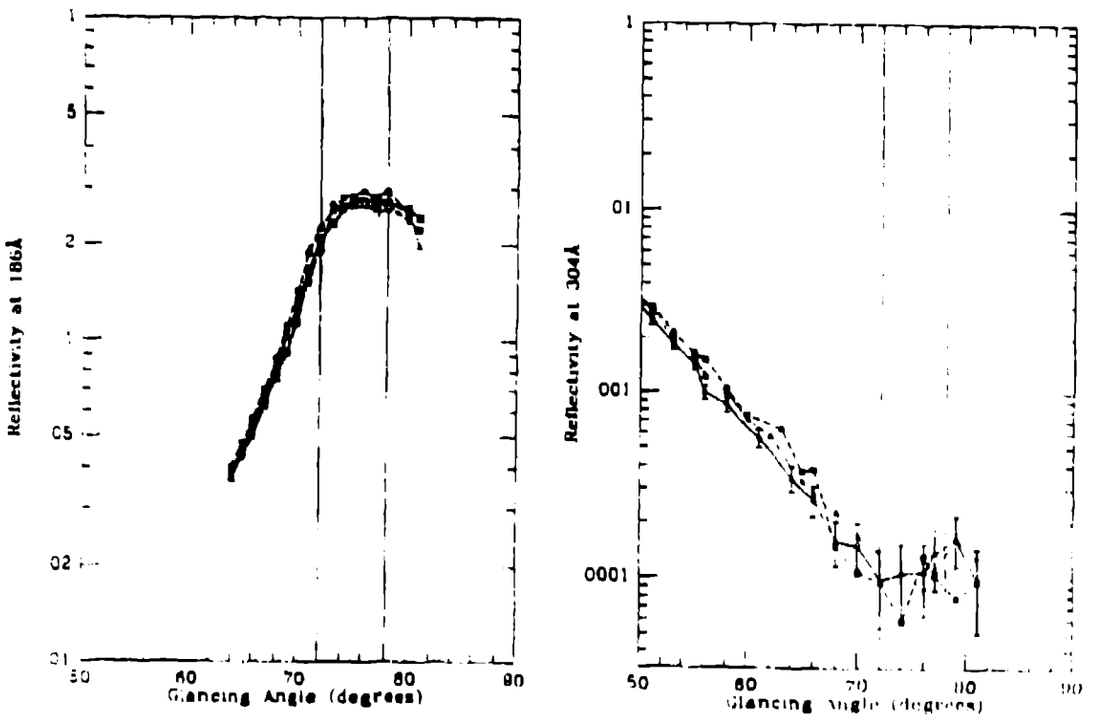

Figure 7. Reflectivity of a 66 eV bandpass flight mirror measured at 186 and 304Å at several mirror radii. The vertical dotted lines indicate the range of reflection angles that any incoming ray could bounce off of the mirror and strike the detector.

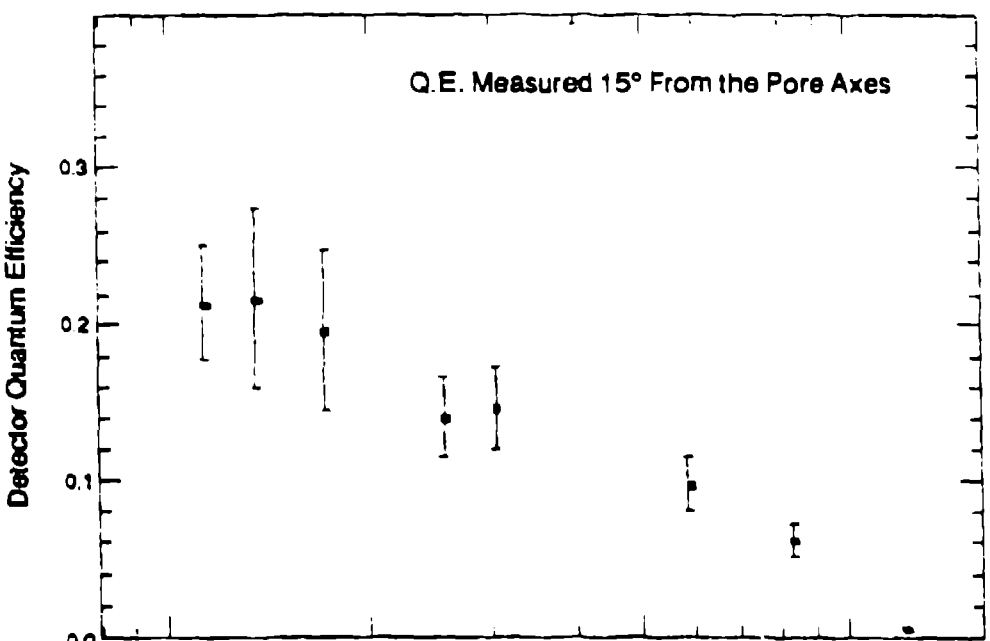

Figure 8. First ALEXIS flight detector quantum efficiency calibration as a function of wavelength.

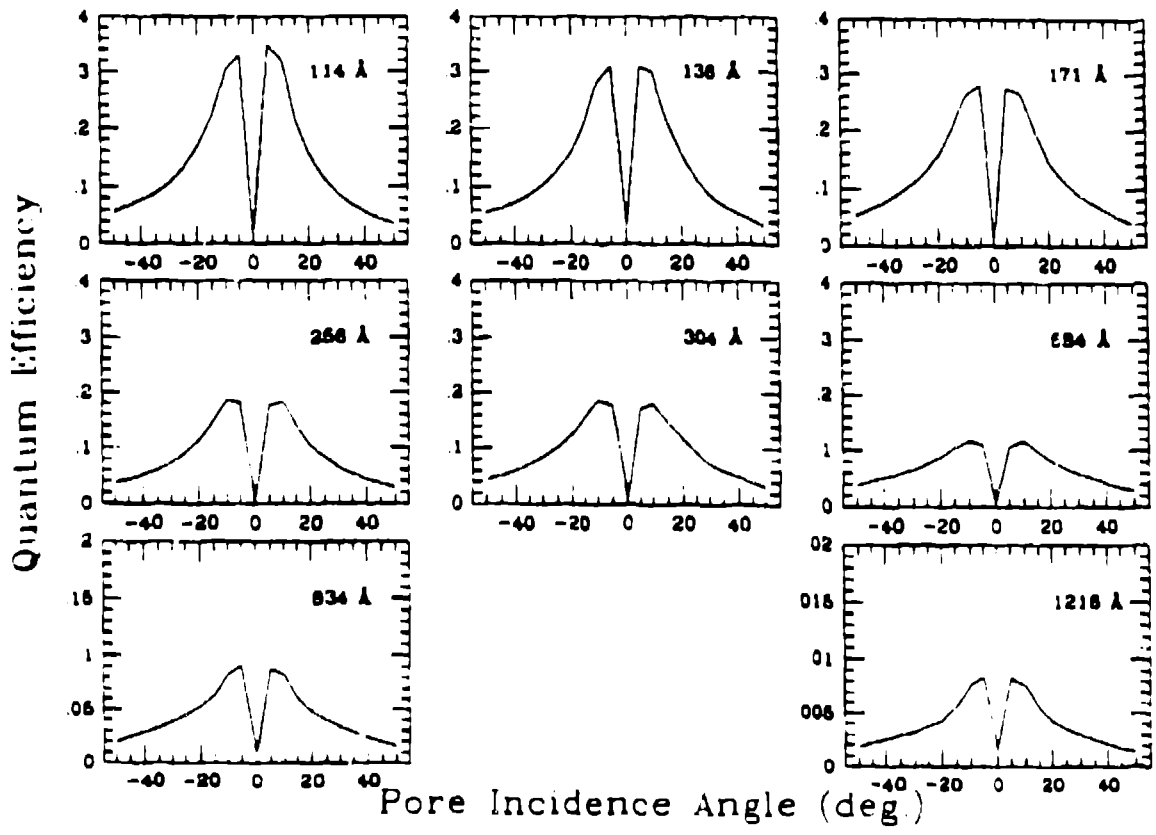

Figure 9. First ALEXIS flight detector Q.E. variations with incident angle at detector center.

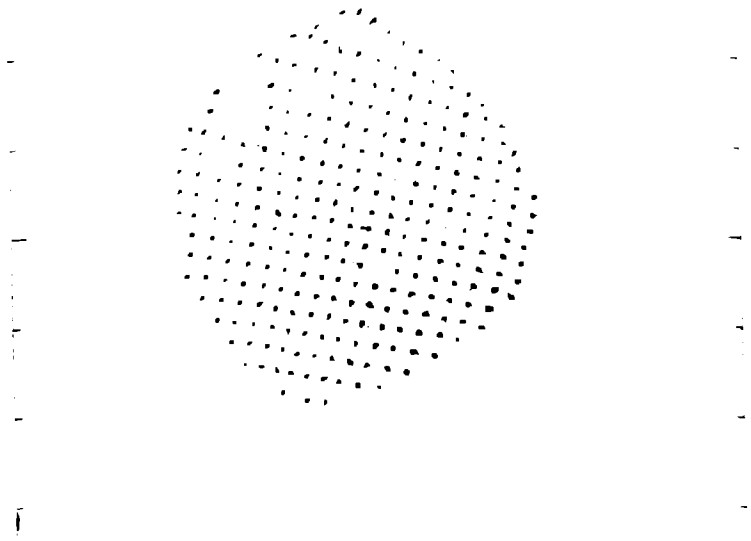

Figure 10. Spatial uniformity test of the first ALEXIS flight detector. This is the image produced when a mask with containing a grid of 2mm spaced 10 micron holes was placed in front of the detector and then illuminated with UV light.

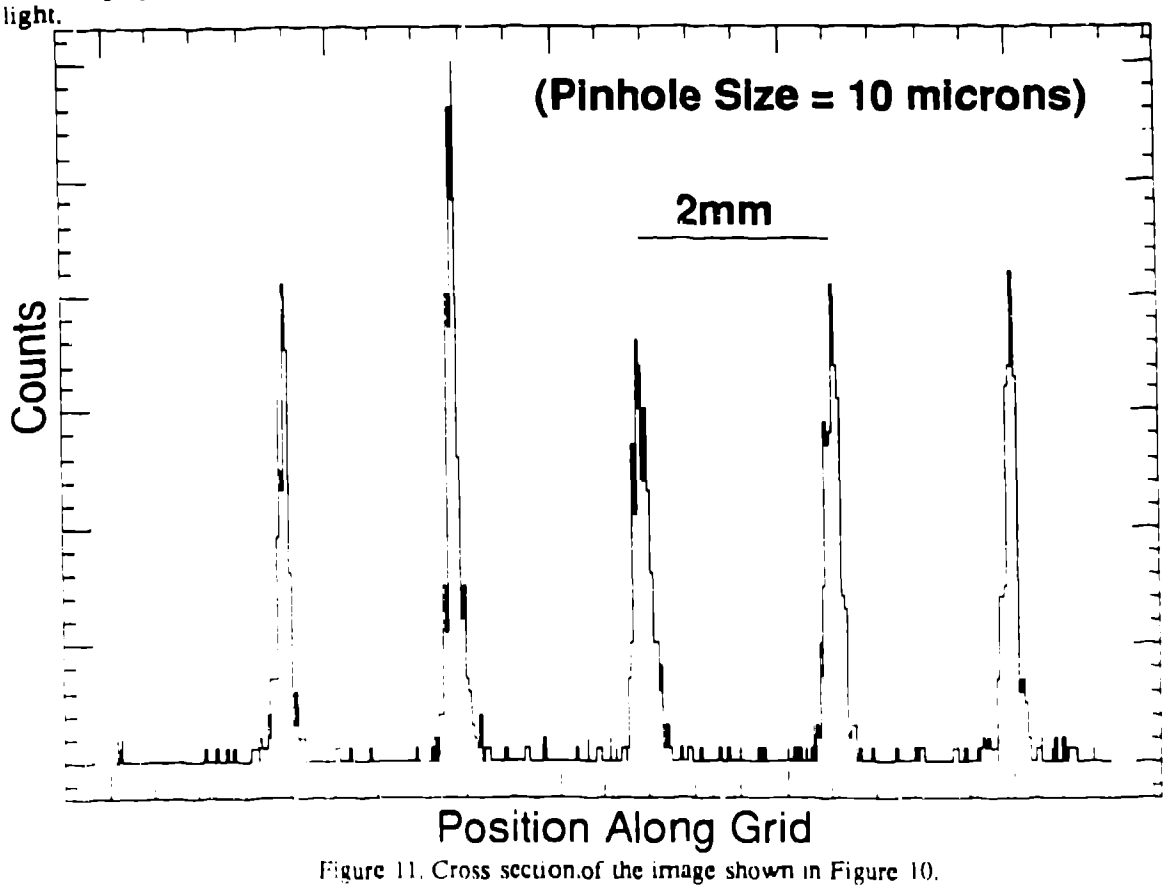

Figure 11. Cross section.of the image shown in Figure 10.

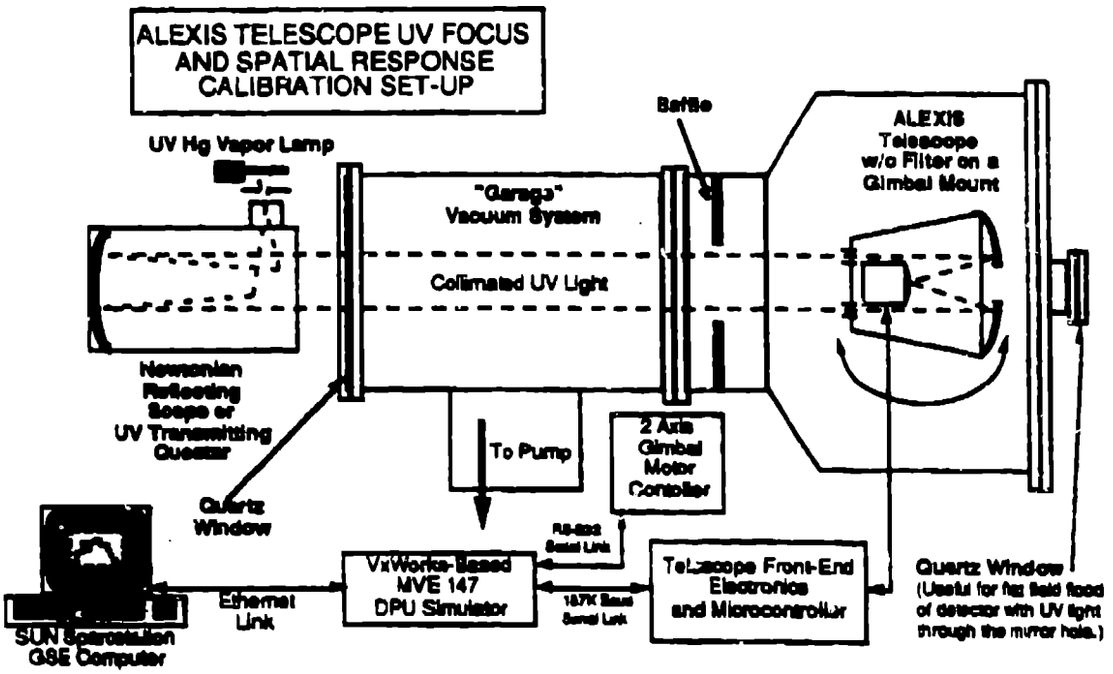

Figure 12. UV focus and spatial calibration test. Its purpose is to measure the point response function of a telescope and map out the relationship between x-y position on the detector and direction in the field of view.

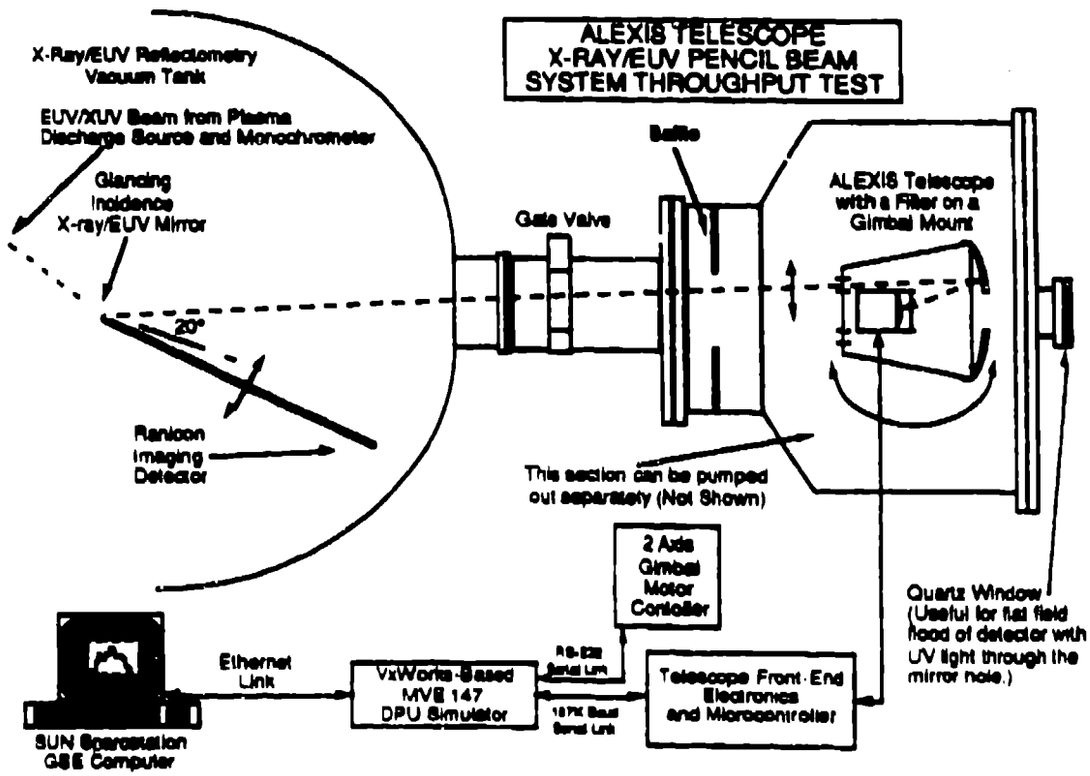

Figure 13. Laboratory Setup for the EUV/X-ray pencil beam test to determine absolute throughput as a function of wavelength. The results are compared with simulations based on the individual wavelength calibrations of the mirror, detector and filter.